Biointerface Research in Applied Chemistry
Open-Access Journal (ISSN: 2069-5837)

Article
Volume 13, Issue 5, 2023, 442
https://doi.org/10.33263/BRIAC135.442

Optimization of the Properties of an Active Oxygen Scavenging POE-Based Nanocomposite Film Reinforced with Graphene and/or Silica using Mixture Design Method for Food Packaging Application

Zhaleh Sheidaei [1], Shervin Ahmadi [2], Mehdi Farhoodi [1,*], Amir Mohammad Mortazavian [1,*], Vahid Mofid [1]

[1] Department of Food Science and Technology, Faculty of Nutrition Sciences and Food Technology, National Nutrition and Food Technology Research Institute, Shahid Beheshti University of Medical Sciences, Tehran, Iran; zhaleh.sheidaei@yahoo.com (Z.S.); farhoodi@sbmu.ac.ir (M.F.); mortazvn@sbmu.ac.ir (A.M.M.); vmofid@sbmu.ac.ir (V.M.);
[2] Iran Polymer and Petrochemical Institute, Tehran, Iran; sh.ahmadi@ippi.ac.ir (S.A.);
* Correspondence: farhoodi@sbmu.ac.ir (M.F.); mortazvn@sbmu.ac.ir (A.M.M.);
Scopus Author ID 57211904446

Received: 29.09.2022; Accepted: 30.10.2022; Published: 20.12.2022

Abstract: The incorporation of iron-based oxygen scavengers into packaging materials is one of the ways that has been used for oxygen-sensitive foods to prolong their shelf life. A well-designed package with oxygen scavenging capability, appropriate gas barrier, and mechanical properties is required. A mixture experimental design was used to develop POE-based nanocomposite films in different proportions of iron-based oxygen scavenger, graphene, and silica nanoparticles. The results pointed out that nanosilica had a reinforcing effect and strengthened the mechanical properties of films. The oxygen scavenging capability and oxygen transmission rate increased at a higher proportion of iron nanoparticles, while graphene and silica had negative effects. According to DSC analysis results, incorporating components into POE resulted in lower melting points and higher crystallization temperatures than neat POE. Nanofiller dispersion was studied by field emission-scanning electron microscopy (FESEM) and X-ray diffraction (XRD). It has been proved that nanocomposite with a mixture of 0.4 wt% iron, 0.3 wt% graphenes, and 0.3 wt% silica showed a uniform dispersion of nanofillers, while with the increase of graphene, aggregation occurred. The optimized formulation obtained was 0.33 wt% iron, 0.21 wt% graphene, and 0.46 wt% silica.

Keywords: Oxygen scavenger, POE, nanocomposite, mixture design

1. Introduction

Consumer demand has shifted to healthy food products with a longer shelf life leading to emerging trends in food packaging technologies. Oxygen deteriorates food quality characteristics by causing many reactions such as fat oxidation, microbial growth, enzymatic browning, and nutrient loss [1]. In order to extend foods' shelf life and customer acceptability, the exclusion of oxygen from packaging is necessary [2]. Modified atmosphere packaging has been developed to maintain the desired quality by modifying the gaseous atmosphere within packages [3, 4]. However, the oxygen remaining inside the package and the oxygen permeating through the package materials, especially materials with an insufficient gas barrier, lead to food deterioration [5]. Another technique for the removal of oxygen is vacuum packaging. It was also found that the vacuum method cannot eliminate the oxygen entering the packaging [6]. Incorporating oxygen scavengers into food packaging structure is one of the most recently used approaches for reducing oxygen or preventing the permeation of it through the packaging material [7, 8]. Integrating nano-sized iron-based oxygen scavenger directly into the packaging film structure or introducing it into various layers of multi-layer packaging film has been commonly used [8]. The multi-layer oxygen scavenging film protected the sausage against oxygen deterioration leading to better quality preservation [9].

A significant feature that determines the product's expected shelf life is the gas permeability of polymeric materials in food packaging [10, 11]. The reinforcement of polymer matrices by nanofillers removes some of their drawbacks associated with a poor gas barrier, and thermal and mechanical properties [12, 13]. The nanoscale fillers provide a large interfacial area, improving various properties of nanocomposites [12]. They lend some properties to polymer matrices, such as enhancing their mechanical strength, thermal stability, and many other properties [14]. For instance, the addition of nanoclay to the PP matrix revealed some noticeable improvements in tensile strength, thermal properties, and oxygen permeability [15, 16].

Polyolefin elastomer (POE) is a relatively new type of copolymer consisting of a larger segment of ethylene and a lower segment of alpha-olefin such as octene, butene, and hexene [17], making it a good option for flexible packaging and other diverse applications [18]. However, POEs' high gas permeability restricts their applications in the packaging industry [19]. Therefore, the incorporation of inorganic fillers into the POE has been developed to improve its performance capabilities [20].

Silica nanoparticles (NPs) have gained much attention for their large surface-to-volume ratio and low toxicity, considering them in the preparation of nanocomposites. Homogeneous dispersion of silica NPs in the polymer matrices significantly affects the performance of the polymer [14]. They improve the polymer's strength, heat resistance, and optical properties [21]. Silica incorporated into PE and PP matrices showed higher tensile strength, modulus, and elongation than PE and PP without nanofiller [22]. The integration of silica NPs into polymers by various approaches offered enhanced mechanical properties [23] and thermal stability of nanocomposite [24].

Graphene, with a high surface area, has been considered a potential material for packaging applications due to its excellent mechanical properties, thermal conductivity, and optical transmittance [25-28]. Graphene and its derivatives significantly impact the polymer's mechanical properties [11, 29, 30]. They make a strong interfacial interaction with the polymer, which influences the thermal characteristics [31]. They can also enhance the oxygen barrier properties of nanocomposites. Adding 0.4 wt% of GO and GNP to the PLA matrix resulted in a threefold reduction in oxygen permeability [32].

It is imperative to use an appropriate way to determine the optimal formulation of an active film. Among all the experimental design methods, the D-Optimal mixture design is the best technique to investigate the optimal formulation of composite materials [33]. Moreover, compared to other methods, it has fewer runs and is more time and cost-effective [34].

The present study aimed to investigate the effects of iron-based oxygen scavenger, silica and graphene nanoparticles on oxygen scavenging capability, oxygen transmission rate, and mechanical properties of active films and to find an optimized formulation using a mixture design method.

2. Materials and Methods

2.1. Materials.

Polyolefin elastomer (POE) (LUCENE LC565) with a density of 0.865 g/cm^3 and melting flow index (MFI) of 5 g/10min (at 190°C) was supplied from LG chem (Seoul, South Korea), POE-*g*-MAH (CMG5805) (Density 0.87-0.9 g/ml, MFI 0.5-2 g/10 min (190 °C, 5 kg)) was obtained from Fine Blend Compatilizer Jiangsu Co., Ltd (China), Fe nanoparticles (Iron, 99.5%, 25 nm, partially passivated) was provided by US Research Nanomaterials, Inc (Houston, USA), nanosilica (> 99.8% SiO_2 content) was obtained from Wacker Chemie AG., (Munich, Germany) and graphene (1µ, 1-2 nm, > 98% pure) was purchased from United Nanotech Innovations Pvt. Ltd (Bangalore, India).

2.2. Methods.

2.2.1. Experimental design.

A mixture design, with constraints on the proportions of the components, was used for film preparation. In this study, the effects of variables concentrations, including iron (0.1-1 wt%), silica (0-1 wt%), and graphene (0-1 wt%) in a mixture of POE + POE-g-MAH (99 wt%) with a fixed proportion of 97:3 (POE: POE-g-MAH) on elongation at break (EB), Young's modulus (YM), tensile strength (TS), oxygen transmission rate (OTR) and oxygen scavenging capability (OSC) were examined. Preliminary tests were used to determine each component's low and high constraints. Table 1 presents the experimental runs in five repetitions given by mixture design. The concentrations of each variable in real and pseudo-component values in different blends are also reported.

Table 1. Real and Pseudo-component values of the independent variables by mixture design.

Sample	**Components**			**Pseudo-components**^{a}		
	Nano-iron	Nano-silica	Nano-graphene	x_1	x_2	x_3
1	0.848	0.000	0.152	0.831	0	0.169
2	1.000	0.000	0.000	1	0	0
3	1.000	0.000	0.000	1	0	0
4	0.100	0.900	0.000	0	1	0
5	0.100	0.443	0.457	0	0.492	0.508
6	0.550	0.450	0.000	0.5	0.5	0
7	0.243	0.600	0.157	0.159	0.667	0.175
8	0.398	0.301	0.302	0.331	0.334	0.335
9	0.100	0.000	0.900	0	0	1
10	0.253	0.147	0.600	0.170	0.164	0.666
11	0.100	0.443	0.457	0	0.492	0.508
12	0.100	0.900	0.000	0	1	0
13	0.550	0.450	0.000	0.5	0.5	0
14	0.698	0.153	0.149	0.665	0.17	0.166
15	0.100	0.000	0.900	0	0	1
16	0.550	0.000	0.450	0.5	0	0.5

x_i shows the pseudo-components values of component: x_1= iron, x_2=graphene, and x_3=silica

2.2.2. Nanocomposite preparation.

POE and POE-g-MAH compatibilizers with different proportions of iron, silica, and graphene nanoparticles were melt-blended using a laboratory twin-screw extruder (model ZSK

25, Werner & Pfleiderer, Germany). The screw diameter (D) and L/D ratio of the extruder were 25 mm of 40/1, respectively. A temperature profile of 130/150/170/170/170 °C was applied, and the rotation speed of the screw was set to 150 rpm. The extruded pellets were placed between two plates of hot-pressed (Mini Test Press Toyo Seiki) at 170 °C and 20 MPa to produce the films. Then the mold was held into a water-cooled hydraulic press to cool it down to room temperature.

2.3 Mechanical properties.

Mechanical properties of POE nanocomposites, including the tensile strength (TS), elongation at break (EB), and Young's modulus (YM), was determined using a Santam STM-50 universal testing machine at a cross-head speed of 500 mm/min at room temperature, according to ASTM D882. Each sample was tested 5 times for tensile properties.

2.4. Oxygen transmission rate.

The oxygen transmission rate (OTR) of the films in cc/ (m^2 day atm) was measured by an Oxtran 100 equipment (Mocon, MN, USA), based on ISO 15105-1/ ASTM standard method D 3985. The OTR test was carried out at 23 ± 2 °C and 80% relative humidity (RH). The thickness of the films was determined by a micrometer (Mitutoyo, Japan). The films were purged by nitrogen and then exposed to oxygen flow. The oxygen gas purity was > 99.5%. The test was performed in triplicate, and the average values were reported.

2.5. Oxygen scavenging capability.

The oxygen absorption capacity of samples was measured by a gas analyzer (Oxybaby®6.0, HTK, Hamburg, Germany). 1 g of the nanocomposite was placed inside a septum-capped vial with a volume of 40 ml at room temperature (24 °C). The relative humidity in vials was kept at 100% and prepared with 1 ml water. The gas analyzer' needle was inserted through the gas-tight septum to measure the headspace oxygen content (%O_2) as a function of time. Gas analyzer calibration was performed in ambient air for each measurement. Each sample was tested three times after 15 days, and the average value was reported as O_2 absorbed/g composite (mL/g).

2.6. DSC.

Differential scanning calorimetry (DSC) test was performed on PerkinElmer DSC- 2C in which the samples were heated first from 0 to 150 °C, maintained for 5 min at 150 °C and then cooled to 0 at a rate of 10 °C/min under the nitrogen purge flow. The degree of crystallinity was obtained from the melting enthalpy of 100% crystalline polyethylene (PE) using the following equation:

$$X_c = \frac{\Delta H_m}{\Delta H_m^0 (1 - \varphi_n)} \times 100$$

where, ΔH_m represents the melting enthalpy from DSC measurements, ΔH_m^0 indicates the melting enthalpy of 100% crystalline PE (290 Jg^{-1}) and φ_n is a weight content of nanofiller.

2.7. FESEM.

Field emission scanning electron microscopy (FESEM) was carried out using a KYKY-EM8000F (China) scanning electron microscope. The surfaces of POE-nanocomposites were coated with gold before being scanned at 20 kV accelerating energy.

2.8. XRD.

X-ray diffraction (XRD) was carried out by Philips X-Pert Pro Diffractometer using Cu K irradiation at a voltage of 45 kV and a current of 40 mA. The data were obtained in the range of 10° to 80° with a step size of 0.02.

2.9. Statistical analysis.

The mechanical properties, oxygen transmission rate, and oxygen scavenging capability of the films were analyzed with Stat-Ease Design Expert 7, Stat-Ease, Inc.). All responses were fitted to quadratic models to explain the relationship between the responses and the factors followed by Eq. 1:

$$y = \beta_1 x_1 + \beta_2 x_2 + \beta_3 x_3 + \beta_{12} x_1 x_2 + \beta_{13} x_1 x_3 + \beta_{23} x_2 x_3$$

where y is the dependent variable, β is the regression coefficient for each component and x_1, x_2 and x_3 represent the levels of iron, graphene, and silica, respectively. Analysis of variance (ANOVA) determined the significance of the fitted model (P-value <0.05 and LOF $>$ 0.05). In order to study the relation between mixture variables and measured responses, the triangular contour plots of the polynomial equation were analyzed. The contour plot helps to visualize changes in a response along with changes in experimental factors. In a contour plot, the contour lines represent the constant responses in a two-dimensional plot [35].

3. Results and Discussion

The mechanical characteristics, OTR, and OSC results of the films are presented in Table 2. The quadratic models were selected as appropriate regression models to predict the effect of each variable on measured responses. Table 3 summarizes the statistical results of ANOVA for TS, EB, YM, OTR, and OSC. It can be seen that the fitted models are highly significant ($p \leq 0.05$), and an insignificant lack of fit is shown for all the studied responses ($p \leq 0.05$). The adjusted regression coefficient (R^2 adj) ranged between 0.94 and 0.99, suggesting that the models predicted the responses adequately.

3.1. Tensile strength.

The tensile strength values of films were between 1.52 and 1.87 Mpa. As seen in Table 3, according to the modeling coefficients, silica had a more coefficient (β 1.84) on TS than the other components. In other words, increasing the amount of silica resulted in strengthened films. The contour plot of TS as a function of the three mixture components (Figure 1a) shows that the inclusion of high values of graphene into POE decreased the TS values. This was owing to the weak interfacial bonding at the interfaces of graphene nanosheet and polymer as well as the agglomeration of graphene [36, 37]. The agglomerates acted as stress concentrators and reduced the TS [11]. As seen from the graph, the addition of nanosilica strengthened the TS in the final nanocomposites (indicated by the red contour), which was attributed to the formation of hydrogen bonds between the anhydride group of POE-g-MAH, as a compatibilizer, and the hydroxyl groups of the silica NPs leading to good interfacial bonding between the filler and polymer [38]. However, the increase in iron and graphene content had a decreasing effect on

TS values (demonstrated by the blue area). The maximum TS was at 0.25 wt% iron, 0.15 wt% graphene, and 0.6 wt% silica. The obtained plot confirms the interaction effects of the nanoparticles in tensile strength.

Table 2. The results of mechanical, OTR and OSC properties of the films.

Run		**Mechanical Properties**[a]		**OTR (cc/ (m^2 day atm))**[a]	**OSC (ml)**[a]
	TS (Mpa)	EB (%)	YM (Mpa)		
1	1.66 ± 0.07	1922.58 ± 15.7	2.03 ± 0.05	1760.19 ± 14.37	8.7 ± 0.07
2	1.55 ± 0.13	1294.13 ± 10.57	1.94 ± 0.02	1948.2 ± 15.91	9.38 ± 0.15
3	1.52 ± 0.04	1218.06 ± 9.95	1.89 ± 0.08	1876.7 ± 15.32	9.29 ± 0.08
4	1.54 ± 0.06	867.46 ± 7.08	1.96 ± 0.06	1228.87 ± 10.03	2.34 ± 0.04
5	1.71 ± 0.1	1733.7 ± 14.16	2.19 ± 0.13	908.93 ± 7.42	2.88 ± 0.02
6	1.66 ± 0.09	1265 ± 10.33	2.14 ± 0.09	1324.09 ± 10.81	3.57 ± 0.06
7	1.71 ± 0.14	1416.27 ± 11.56	2.09 ± 0.07	1057.92 ± 8.64	2.98 ± 0.05
8	1.81 ± 0.15	1816.23 ± 14.83	2.21 ± 0.05	1125.94 ± 9.19	4.32 ± 0.07
9	1.84 ± 0.05	1937.08 ± 15.82	2.3 ± 0.02	1644.88 ± 13.43	3.21 ± 0.03
10	1.87 ± 0.08	2023.02 ± 16.52	2.23 ± 0.16	1392.24 ± 11.37	4.24 ± 0.07
11	1.78 ± 0.13	1637.33 ± 13.37	2.18 ± 0.09	946.93 ± 7.73	2.4 ± 0.04
12	1.59 ± 0.04	879.76 ± 7.18	1.96 ± 0.11	1289.37 ± 10.53	2.52 ± 0.02
13	1.66 ± 0.12	1112.4 ± 9.08	2.07 ± 0.15	1374.59 ± 11.22	3.43 ± 0.03
14	1.7 ± 0.07	1668.66 ± 13.62	2.08 ± 0.07	1498.02 ± 12.23	6.44 ± 0.11
15	1.84 ± 0.11	1855.72 ± 15.15	2.27 ± 0.06	1651.88 ± 13.49	3 ± 0.05
16	1.79 ± 0.04	2100.42 ± 17.14	2.15 ± 0.12	1624.74 ± 13.27	7.03 ± 0.06

[a] Each value is the mean of three measures ± SD.

Table 3. Best adjusted model and goodness of fit obtained for the mechanical, OTR and OS properties.

Response	**F-value**	***p*-value**	**Lack of fit (*p*)**	**R^2**	**Adj R^2**	**Model**
TS	50.25	< 0.0001	0.6076	0.9617	0.9426	+ 1.53A + 1.56B + 1.84C + 0.49AB + 0.52AC + 0.22BC
EB	65.05	< 0.0001	0.2044	0.9702	0.9553	+ 1303.04A + 879.07B + 1882.08C + 422.56AB + 2427.92AC + 1219.16BC
YM	71.44	< 0.0001	0.7681	0.9728	0.9592	+ 1.92A + 1.96B + 2.28C + 0.66AB + 0.24AC + 0.24BC
OTR	155.30	< 0.0001	0.2289	0.9873	0.9809	+ 1905.94A + 1258.26B + 1663.33C - 983.99AB -650.65AC - 2131.11BC
OSC	746.06	< 0.0001	0.7297	0.9973	0.9960	+ 9.30A + 2.45B + 3.10C - 9.25AB + 3.52AC - 0.24BC

A (iron), B (graphene), C (silica) expressed as pseudocomponents. TS: tensile strength; EB: elongation at break; YM: Young modulus; OTR: oxygen transmission rate; OS: oxygen scavenging.

3.2. Young's modulus.

Young's modulus is related to the rigidity of the packaging material. The YM values of the nanocomposites varied between 1.89 and 2.3 Mpa. The stiffness of the polymer matrix increased with the reinforcing effect of silica NPs [39], which could be the reason for the greatest coefficient observed for silica (β 2.28) (Table 3). The contour plot of the YM at different levels of nanoparticles is shown in Figure 1b. As seen, the maximum YM was obtained at the lowest levels of graphene (0 wt%) and iron (0.1wt%), while silica was in its highest level (0.9 wt%). It is evident that the presence of silica had an obvious effect on YM; therefore, with increasing the content of which, the red areas indicating the highest YM values went up. It seems that the uneven dispersion and lower interfacial adhesion of graphene nanoplatelets/polymer matrix have led to a decrease in YM [40-42].

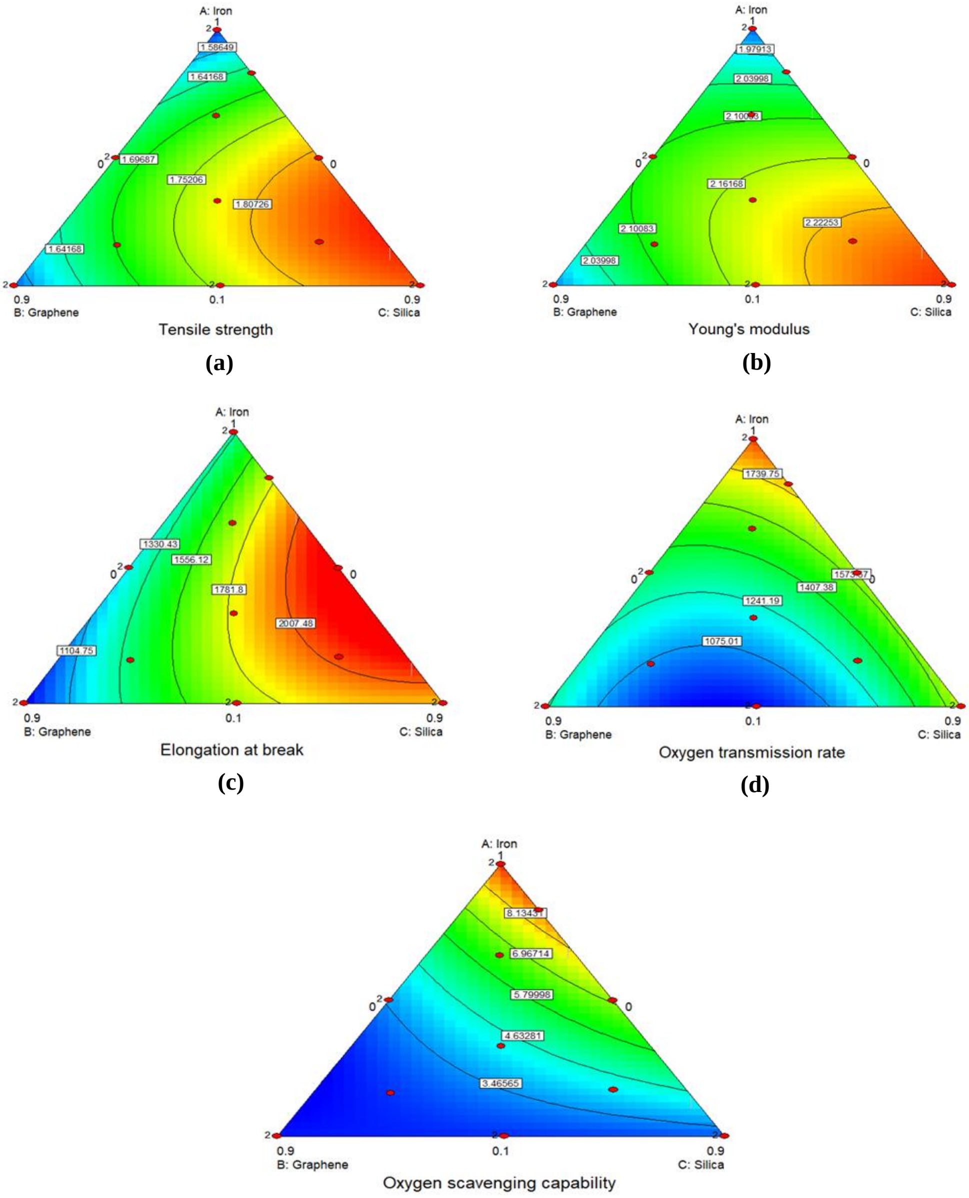

(a) **(b)**

(c) **(d)**

(e)

Figure 1. Surface contour plot for **(a)** tensile strength; **(b)** Young's modulus; **(c)** elongation at break; **(d)** oxygen transmission rate; **(e)** oxygen scavenging capability.

3.3. Elongation at the break.

Considering the regression coefficients of graphene (β 879.07) and silica (β 1882.08), the introduction of graphene into the composite restricted the movement of the polymer chains; thus, they could not dissipate the applied mechanical energy [43]. With the growing incorporation of graphene, the ductility of the polymer phase decreased, and poor interfacial adhesion of graphene/POE resulted in a reduction in elongation at break (Table 2) [44, 45]. This is in contrast with the findings of Krystyjan, Khachatryan [46]. However, when silica nanoparticles were added, the surface bonding between the polymer molecules increased. This is why the elongation at break values of the nanocomposite increased [47]. Figure 1c shows the interaction effect of mixture constituents on the elongation at break. It is clear that with increasing amounts of graphene in the mixture, EB shifted to lower values demonstrated by the increased blue areas in the plot. This could be explained by improper distribution, and agglomeration of this component reduced the EB of the nanocomposites.

3.4. OTR.

In order to test the OTR of the films, their passive function in inactive mode was evaluated. The oxygen scavenger nanocomposites were inactivated by placing them in ambient conditions until no oxygen absorption occurred. According to the results (Table 3), nano iron presented the highest coefficient (β 1905.94) with the most pronounced influence on OTR. This can be ascribed to forming small pores in the polymer matrix by iron NPs [48]. The free volume created in the composite structure led to an increase in oxygen permeability [49]. The binary interaction coefficient of BC was the highest, giving more evidence of the barrier effects of graphene and silica. As seen in Table 2, the treatment with 0.1 wt% iron, 0.45 wt% graphene, and 0.45 wt% silica showed the lowest OTR (1817 cc/ (m2 day atm). Adding graphene to POE nanocomposites decreased OTR values since graphene platelets created a tortuous permeation path that acted as a gas barrier [50]. This agrees with the findings from [7, 51, 52]. Khalaj, Ahmadi [53]. They found that clay platelets, as a physical barrier, slowed down the permeation of oxygen through the polymeric film and increased the distance of oxygen passing across the polymeric matrix. The contour plot of OTR for POE-based nanocomposites at various combinations of components is shown in Figure 1d. The plot depicted that OTR decreased with an increase in graphene and silica contents showing their barrier effects on oxygen permeation [54].

3.5. Oxygen scavenging capability.

The adjusted model showed that nano iron with the highest linear coefficient greatly impacted the oxygen absorption results (Table 3). The negative interaction coefficient term of AB stated that iron, in combination with graphene, exerted an antagonist effect on the response. The oxygen scavenging capability of POE nanocomposites at 24 °C and 100% RH are reported in Table 2. High humidity acted as an activator that stimulated the oxygen absorption of films. After 15 days, the highest oxygen absorption (2.38 ml/g composite) was observed for sample with high proportions of iron (1 wt%), whereas the composite with 0.1 wt% iron and 0.9 wt% graphene showed the lowest oxygen absorption (2.34 ml/g composite). This is consistent with the conclusions reported by Gibis and Rieblinger [9]. The integration of an iron-based oxygen scavenger into packaging material (EVA polymer) led to significant improvements in the oxygen consumption of sausage when exposed to light [9]. The Iron kaolinite incorporated into LLDPE and HDPE matrices absorbed 4.3 ml and 2.4 ml oxygen/g composite, respectively, after 60 days (at 24 °C and 100% RH) [7]. Galdi, Nicolais [55] studied the performance of the 5% Amosorb as an oxygen scavenger added to PET. They reported that all active films scavenged 0.81 to 0.86 ml of oxygen per gram of composites, however after 26 hours, the Amosorb activity reached a plateau level. The OSC of iron-based oxygen scavenger added to fish gelatin film was evaluated [56]. The active film had an oxygen scavenging capacity of 1969.08 ml O_2/m^2/mil in the presence of moisture after 50 days. It has been reported [7] that the ability of oxygen to bind to iron centers in the nanocomposite structure determines the oxygen-scavenging capability of the composite. As a result, the film with 1 wt% nano iron showed the highest permeability to oxygen and moisture and scavenged the oxygen effectively. Figure 1e indicates that graphene and silica reduced the oxygen scavenging value of composites to a lower extent, which was mainly related to the barrier effects of nanofillers.

3.6. DSC.

DSC measurements were carried out to determine any changes in melting and crystallization temperatures (Tm and Tc), melting and crystallization enthalpies (ΔHm and ΔHc), and crystallinity degree (Xc%) in the nanocomposites (Figure 2). The melting temperature of pure POE (control) was 49.08 °C (Table 4). The addition of nano iron to POE decreased the melting temperature to 47.27 °C (T2). Graphene and/or silica NPs have also caused a drop in melting temperature to 45.93 °C (T3), 46.76 °C (T7), and 45.75 °C (T8). The crystallization behavior of samples showed that incorporating nanocompounds into POE increased crystallization temperatures except for T8 (Figure 2b). The treatment containing 0.9 wt% graphene (T3) showed maximum Tc since the additional graphene incorporation formed aggregates that acted as nucleating agents. Results are consistent with those of other studies [57, 58]. Tesarikova and Merinska [59] suggested that the increase in Tc of EOC/ Cloisite 93 was due to the lower mobility of polymer chains after the addition of nanofillers. However, this differs from the reported data by Gaska and Xu [60], in which case, a Tc decrease of LDPE/graphene composite was owing to good dispersion of nanofiller that prevented the growth of LDPE crystallites. It can be seen from Table 4 that the introduction of 0.9 wt% nanosilica (T8) decreased the crystallization temperature to 18.91 °C, which affirmed the anti-nucleation behavior. As the properties of the nanocomposites are widely dependent on polymer/filler interactions [61], adding silica in the presence of POE g-MAH led to more finely dispersed nanocomposites due to the improved polymer/nanofiller interactions. The degree of crystallinity of nanocomposites decreased, starting from 7.17 % for pure POE to a minimum of 4.1 % for T3. The observed reduction was attributed to the fact that the nanofillers reduced the continuity of the polymer matrix, especially plate-like nanofillers incorporation decreased the level of crystallinity in thermoplastic nanocomposites [62]. This is consistent with the conclusions from Tarani and Papageorgiou [62] for LDPE/GNP nanocomposites.

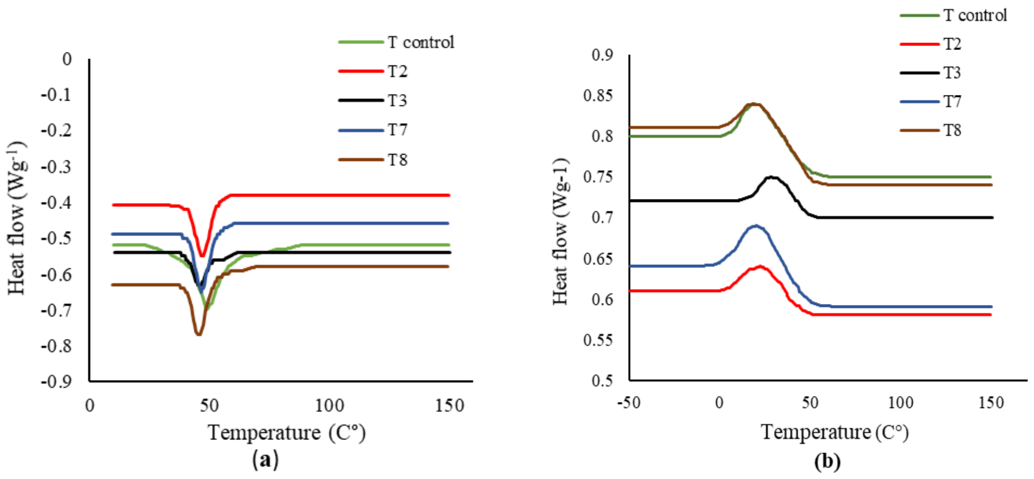

Figure 2. DSC thermograms of POE-based nanocomposites during **(a)** heating and **(b)** cooling**.**

Table 4. Differential scanning calorimetry results of selected POE-based nanocomposites.

Sample	**T_m (° C)**	**T_c (° C)**	**X_c (%)**	**ΔH_m (J.g^{-1})**	**ΔH_c (J.g^{-1})**
Control	49.08	19.25	7.17	20.8	17.08
T2	47.27	22.73	4.69	13.62	12.5
T3	45.93	28.41	4.1	11.9	14.9
T7	46.76	20.90	4.84	14.04	17.08
T8	45.75	18.91	4.51	13.08	13.62

3.7. FESEM.

The dispersion of nanofillers in a polymer matrix has been assessed through microscopic investigations. The surface morphology of nanocomposites of T3, T4, T7, and T8 is shown in Fig. 3. A comparison of the graphene distribution in a matrix of POE can be seen in Figs. 3a-e. Fig. 3e confirms the uniformity of graphene nanosheet distribution as well as an appropriate silica/polymer interfacial interaction. In this treatment, any agglomerated structures of graphene have not been observed, suggesting the polymer chains intercalated into graphene interlayers. It comes from Figs. 3a-d that T3 and T4 morphology consisted of randomly aggregated sheets of graphene associated closely with each other. This reveals that higher graphene concentrations (0.44 wt% and 0.9 wt%) gave a comparatively rough surface to nanocomposites which are attributed to the nanofillers agglomeration (Fig. 3a-3d). This is in agreement with the conclusions from the XRD analysis. It can be seen from Fig. 3f that silica NPs were dispersed uniformly in the POE matrix. The compatibility of the POE with silica was due to the incorporation of POE-g MAH into the polymer chains. The compatibilizer reduced the interfacial tension between the non-polar POE and polar nanosilica, making a much finer morphology.

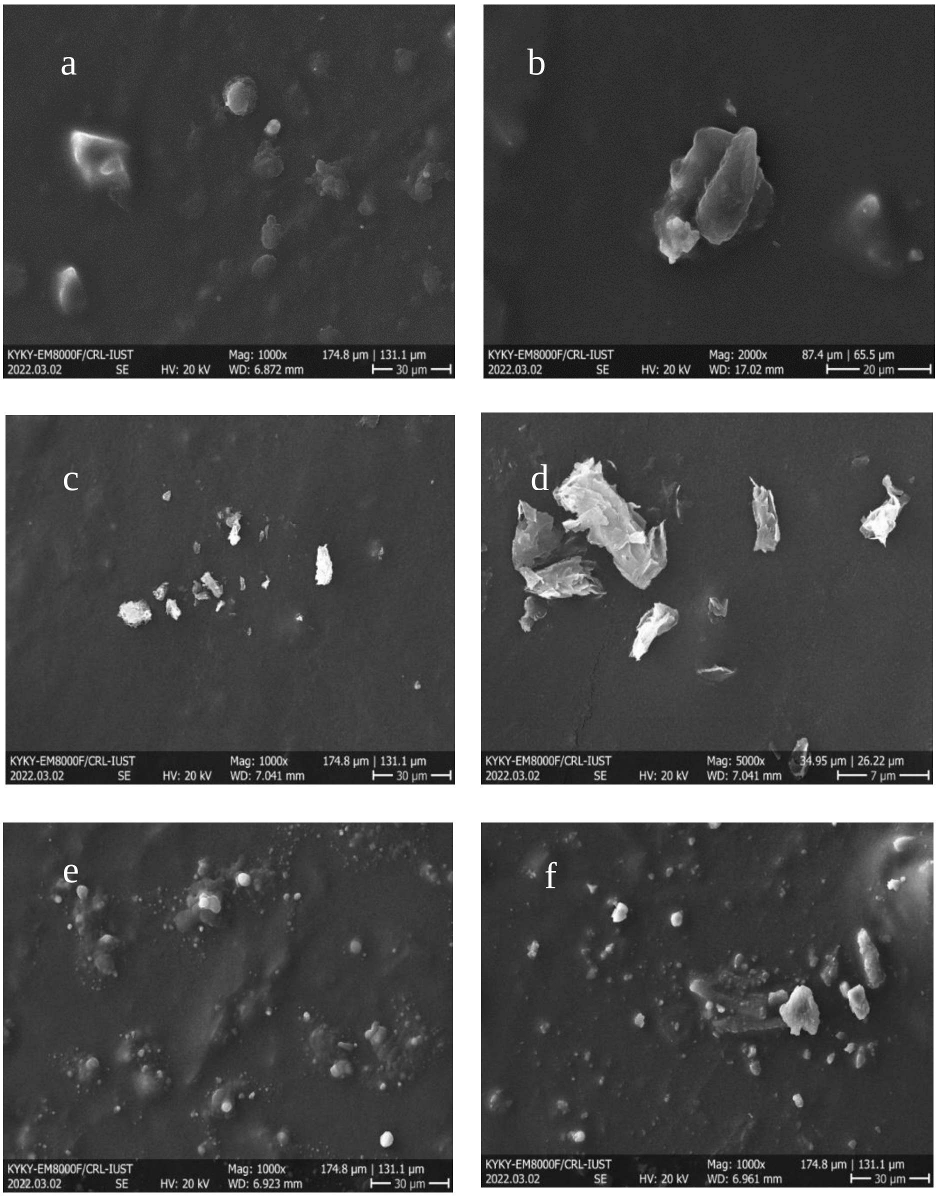

Figure 3. Fe-Sem images of POE nanocomposites. **(a)** and **(b)** T3; **(c)** and **(d)** T4**; (e)** T7 and **(f)** T8.

3.8. XRD

XRD analysis was carried out to investigate the presence of graphene in nanocomposites. XRD patterns of pure POE, graphene, and their nanocomposite (T3) have been compared (Fig. 4). The diffraction peak of graphene appeared at 26.5° corresponding to the d spacing value of 3.37 nm, and the spectrum of pure POE showed a peak at 19.2 ° (Table 5). Fig. 4 confirmed the difference between the curves of POE/graphene composite and pure POE. A remarkable peak at 2θ ~ 26.4° representing the distance between the graphene layers was observed in POE/graphene composite. As seen in Figure 4, a small shift in the diffraction peak of graphene occurred towards lower angles from 26.5° to 26.4°. This can be concluded that the distance between the graphene plates did not change significantly, which can be interpreted as an agglomeration of graphene nanoplatelets at 9 wt%. In addition, graphene inclusion decreased the diffraction peak's intensity, causing a decrease in the crystallinity of the nanocomposite. However, Sabet and Soleimani [54] reported that the peak intensity arose with the additional graphene in LDPE.

Table 5. XRD parameters of nanocomposite films.

Treatment	**Peak angle, 2θ (°)**	**Interlayer distance (nm)**
Pure POE	19.198	4.61
Graphene	26.475	3.37
T3	26.395	3.38

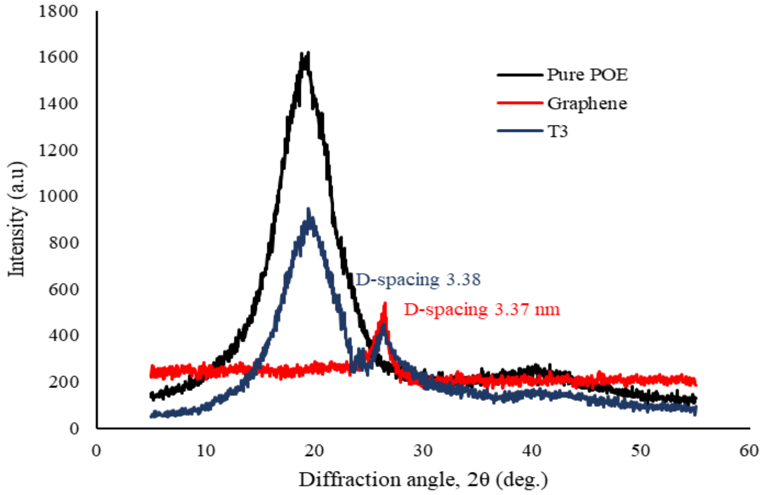

Figure 4. XRD graphs of pure POE, graphene, and T3.

3.9. Optimization of the variables

To optimize multiple responses, the constraints of iron, silica, and graphene values were set within the range, the EB, YM, TS, and OSC were set to maximum, and OTR was defined as the minimum. The propagation of error (POE) values were set to a minimum to provide a more robust design. The final optimized formulation was found to be 0.33 wt% iron, 0.21 wt% graphene, and 0.46 wt% silica, with a maximum desirability of 0.762. In order to validate the adequacy of the model equations, verification experiments were carried out in triplicate. The predicted and experimental results for the optimal formulation are reported in Table 6. As seen, the data predicted by models were in good agreement with the experimental results ($p > 0.05$).

Table 6. Predicted and experimental values of responses for optimal combination.

Responses	**Predicted value**	**Experimental value**	**P (T ≤ t) two-tail**
TS	1.81 ± 0.01	1.85 ± 0.04	0.15

Responses	Predicted value	Experimental value	P (T ≤ t) two-tail
YM	2.2 ± 0.01	2.22 ± 0.02	0.07
EAB	1951.56 ± 38.15	1967.25 ± 53	0.21
OTR	1199.24 ± 19.78	1221.41 ± 32.28	0.09
OS	4.26 ± 0.07	4.3 ± 0.04	0.27

4. Conclusions

POE/POE-g-MAH nanocomposites incorporated with different contents of iron, silica, and graphene nanoparticles were produced by the melt blending process. The mixture experimental design effectively determined the effects of different variables on nanocomposite properties and proposed an optimized formulation. Nanosilica proved as a good reinforcing filler even at high concentrations and enhanced the mechanical properties of the films. Graphene and silica nanofillers contributed to the improvement of oxygen barrier properties, while these components had a negative effect on oxygen scavenging capacity. The optimum conditions were found to be 0.33 wt% for iron, 0.21 wt% for graphene, and 0.46 wt% for silica. It can be concluded that the produced oxygen scavenging film with improved physical properties gives the best performance in food packaging applications.

Funding

This research received no external funding.

Acknowledgments

We are grateful to the Department of Food Science and Technology, National Nutrition and Food Technology Research Institute (Shahid Beheshti University of Medical Sciences) for support of this study.

Conflicts of Interest

There is no conflict of interest to report. All authors have participated in the design or analysis of the data, revising the article for important intellectual content, and approved of the final version.

References

1. Promsorn, J.; Harnkarnsujarit, N. Pyrogallol loaded thermoplastic cassava starch based films as bio-based oxygen scavengers. *Industrial Crops and Products* **2022**, *186*, 115226, https://doi.org/10.1016/j.indcrop.2022.115226.
2. Cichello, S.A. Oxygen absorbers in food preservation: a review. *Journal of food science and technology* **2015**, *52*, 1889-1895, https://doi.org/10.1007/s13197-014-1265-2.
3. Sandhya,. Modified atmosphere packaging of fresh produce: Current status and future needs. *LWT-Food Science and Technology* **2010**, *43*, 381-392, https://doi.org/10.1016/j.lwt.2009.05.018.
4. Manolopoulou, E.; Varzakas, T. Effect of modified atmosphere packaging (MAP) on the quality of 'ready-to-eat'shredded cabbage. *International Journal of Agricultural and Food Research* **2013**, *2*, https://doi.org/10.24102/ijafr.v2i3.269.
5. Foltynowicz, Z. Nanoiron-Based Composite Oxygen Scavengers for Food Packaging, In Composites Materials for Food Packaging. Cirillo, G., Kozłowski, M.A., Spizzirri, U.G., Eds.; John Wiley and Sons, Inc.: New Jersey, USA, **2018**, 209-234, https://doi.org/10.1002/9781119160243.ch6.
6. Byun, Y.; Darby, D.; Cooksey, K.; Dawson, P.; Whiteside, S. Development of oxygen scavenging system containing a natural free radical scavenger and a transition metal. *Food chemistry* **2011**, *124*, 615-619, https://doi.org/10.1016/j.foodchem.2010.06.084.

7. Busolo, M.A.; Lagaron, J.M. Oxygen scavenging polyolefin nanocomposite films containing an iron modified kaolinite of interest in active food packaging applications. *Innovative Food Science & Emerging Technologies* **2012**, *16*, 211-217, https://doi.org/10.1016/j.ifset.2012.06.008.
8. Galotto, M.; Anfossi, S.; Guarda, A. Oxygen absorption kinetics of sheets and films containing a commercial iron-based oxygen scavenger. *Food science and technology international* **2009**, *15*, 159-168, https://doi.org/10.1177/1082013208106207.
9. Gibis, D.; Rieblinger, K. Oxygen scavenging films for food application. *Procedia Food Science* **2011**, *1*, 229-234, https://doi.org/10.1016/j.profoo.2011.09.036.
10. Emblem, A. Plastics properties for packaging materials, In Packaging Technology, Emblem, A., Emblem, H. Eds.; Woodhead Publishing: Cambridge, UK, **2012**, 287-309, https://doi.org/10.1533/9780857095701.2.287.
11. Ahmed, J. Use of Graphene/Graphene Oxide in Food Packaging Materials: Thermomechanical, Structural and Barrier Properties. In Reference Module in Food Science. Smithers, G. Ed.; *Elsevier: Amsterdam, Netherlands* **2019**, http://dx.doi.org/10.1016/B978-0-08-100596-5.22499-2.
12. Fu, S.; Sun, Z.; Huang, P.; Li, Y.; Hu, N. Some basic aspects of polymer nanocomposites: A critical review. *Nano Materials Science* **2019**, *1*, 2-30, https://doi.org/10.1016/j.nanoms.2019.02.006.
13. Singh, T.; Gangil, B.; Ranakoti, L.; Joshi, A. Effect of silica nanoparticles on physical, mechanical, and wear properties of natural fiber reinforced polymer composites. *Polymer Composites* **2021**, *42*, 2396-2407, https://doi.org/10.1002/pc.25986.
14. Rahman, I.A.; Padavettan, V. Synthesis of silica nanoparticles by sol-gel: size-dependent properties, surface modification, and applications in silica-polymer nanocomposites—a review. *Journal of Nanomaterials* **2012**, https://doi.org/10.1155/2012/132424.
15. Choi, R.N.; Cheigh, C.I; Lee, S.Y.; Chung, M.S. Preparation and properties of polypropylene/clay nanocomposites for food packaging. *Journal of food science* **2011**, *76*, N62-N67, https://doi.org/10.1111/j.1750-3841.2011.02351.x.
16. Lee, S., Kang, IA.; Doh, G.H.; Kim, W.J.; Kim, J.S.; Yoon, H.G.; Wu, Q. Thermal, mechanical and morphological properties of polypropylene/clay/wood flour nanocomposites. *Express Polymer Letters* **2008**, *2*, 78-87, https://doi.org/10.3144/expresspolymlett.2008.11.
17. Kontopoulou, M.; Wang, W.; Gopakumar, T. G.; Cheung, C. Effect of composition and comonomer type on the rheology, morphology and properties of ethylene-α-olefin copolymer/polypropylene blends. *Polymer* **2003**, *44*, 7495-7504, https://doi.org/10.1016/j.polymer.2003.08.043.
18. Sadiku, E. Automotive components composed of polyolefins, In Polyolefin Fibres, Ugbolue S.C.O., Ed.; Woodhead Publishing: Cambridge, UK, **2009**, 81-132, https://doi.org/10.1533/9781845695552.1.81.
19. Fujiyama-Novak, J.; Rufino, V.; Amaral, R.; Habert, A.; Borges, C.; Mano, B. Oxygen Permeability of Nanocomposite-Based Polyolefin Films. *Macromolecular Symposia* **2016**, *368*, 19-23, https://doi.org/10.1002/masy.201600001.
20. Wu, C.S.; Liao, H.T. Modification of polyethylene–octene elastomer by silica through a sol–gel process. *Journal of applied polymer science* **2003**, *88*, 966-972, https://doi.org/10.1002/app.11725.
21. Hafttananian, N.; Zabihzadeh Khajavi, M.; Farhoodi, M.; Jahanbin, K.; Ebrahimi Pure, A. Migration of nano-clay and nano-silica from low-density polyethylene nanocomposites into different food simulants. *Journal of Food Measurement and Characterization* **2021**, *15*, 3893-3900, https://doi.org/10.1007/s11694-021-00972-0.
22. Agag, T.; Koga, T.; Takeichi, T. Studies on thermal and mechanical properties of polyimide–clay nanocomposites. *Polymer* **2001**, *42*, 3399-3408, https://doi.org/10.1016/S0032-3861(00)00824-7.
23. Dong, W.; Su, J.; Chen, Y.; Xu, D.; Cheng, L.; Mao, L.; Gao, Y.; Yuan, F. Characterization and antioxidant properties of chitosan film incorporated with modified silica nanoparticles as an active food packaging. *Food Chemistry* **2022**, *373*, 131414, https://doi.org/10.1016/j.foodchem.2021.131414. https://doi.org/10.1016/j.foodchem.2021.131414.
24. Kaseem, M.; Ur Rehman, Z.; Hossain, S.; Singh, A. K.; Dikici, B. A Review on Synthesis, Properties, and Applications of Polylactic Acid/Silica Composites. *Polymers* **2021**, *13*, 3036, https://doi.org/10.3390/polym13183036.
25. Morozov, S.V.; Novoselov, K.S.; Katsnelson, M.I.; Schedin, F.; Elias, DC.; Jaszczak, J. A.; Geim, A.K. Giant intrinsic carrier mobilities in graphene and its bilayer. *Physical review letters* **2008**, *100*, 016602, https://doi.org/10.1103/PhysRevLett.100.016602.
26. Szeluga, U.; Pusz, S.; Kumanek, B.; Olszowska, K.; Kobyliukh, A.; Trzebicka, B. Effect of graphene filler structure on electrical, thermal, mechanical, and fire retardant properties of epoxy-graphene nanocomposites-

a review. *Critical Reviews in Solid State and Materials Sciences* **2021**, *46*, 152-187, https://doi.org/10.1080/10408436.2019.1708702.

27. Kumar, A.; Sharma, K.; Dixit, A.R. A review on the mechanical properties of polymer composites reinforced by carbon nanotubes and graphene. *Carbon Letters* **2021**, *31*, 149-165, https://doi.org/10.1007/s42823-020-00161-x.
28. Santana, J. G.; Akbulut, M.; Temperini, M. L. A.; Rangari, V. K.; Güven, O.; Moura, E. Synergistic effect of e-beam irradiation and graphene oxide incorporation on thermal, mechanical, and barrier properties of poly (ethylene-co-vinyl alcohol) film. *Radiation Physics and Chemistry* **2022**, *199*, 110343, https://doi.org/10.1016/j.radphyschem.2022.110343.
29. Ibrahim, A.; Klopocinska, A.; Horvat, K.; Abdel Hamid, Z. Graphene-Based Nanocomposites: Synthesis, Mechanical Properties, and Characterizations. *Polymers* **2021**, *13*, 2869, https://doi.org/10.3390/polym13172869.
30. Gürler, N.; Torğut, G. Graphene-reinforced potato starch composite films: Improvement of mechanical, barrier and electrical properties. *Polymer Composites* **2021**, *42*, 173-180, https://doi.org/10.1002/pc.25816.
31. Liao, W-H.; Yang, S-Y.; Wang, J-Y.; Tien, H-W.; Hsiao, S-T.; Wang, Y-S.; Li, S-M.; Ma, C-C M.; Wu, Y-F. Effect of molecular chain length on the mechanical and thermal properties of amine-functionalized graphene oxide/polyimide composite films prepared by in situ polymerization. *ACS applied materials & interfaces* **2013**, *5*, 869-877, https://doi.org/10.1021/am302494c.
32. Pinto, A. M.; Cabral, J.; Tanaka, D. A. P.; Mendes, A. M.; Magalhães, F. D. Effect of incorporation of graphene oxide and graphene nanoplatelets on mechanical and gas permeability properties of poly (lactic acid) films. *Polymer International* **2013**, *62*, 33-40, https://doi.org/10.1002/pi.4290.
33. Sarteshnizi, R. A.; Hosseini, H.; Bondarianzadeh, D.; Colmenero, F. J. Optimization of prebiotic sausage formulation: Effect of using β-glucan and resistant starch by D-optimal mixture design approach. *LWT-Food Science and Technology* **2015**, *62*, 704-710, https://doi.org/10.1016/j.lwt.2014.05.014.
34. Zen, N. I.; Abd Gani, S. S.; Shamsudin, R.; Masoumi, H. R.The Use of D-Optimal Mixture Design in Optimizing Development of Okara Tablet Formulation as a Dietary Supplement. *Scientific World Journal* **2015**, 684319, https://doi.org/10.1155/2015/684319.
35. Kim, H. K.; Kim, J. G.; Cho, J. D.; Hong, J. W. Optimization and characterization of UV-curable adhesives for optical communications by response surface methodology. *Polymer Testing* **2003**, *22*, 899-906, https://doi.org/10.1016/S0142-9418(03)00038-2
36. Yasmin, A.; Luo, J.-J.; Daniel, I.M. Processing of expanded graphite reinforced polymer nanocomposites. *Composites Science and Technology* **2006**, *66*, 1182-1189, https://doi.org/10.1016/j.compscitech.2005.10.014.
37. Maniadi, A.; Vamvakaki, M.; Suchea, M.; Tudose, I. V.; Popescu, M.; Romanitan, C.; Pachiu, C.; Ionescu, O. N.; Viskadourakis, Z.; Kenanakis, G.; Koudoumas, E. Effect of Graphene Nanoplatelets on the Structure, the Morphology, and the Dielectric Behavior of Low-Density Polyethylene Nanocomposites. *Materials* **2020**, *13*, 4776, https://doi.org/10.3390/ma13214776.
38. Sadik, W. A. A.; El Demerdash, A. G. M.; Abbas, R.; Bedir, A. Effect of Nanosilica and Nanoclay on the Mechanical, Physical, and Morphological Properties of Recycled Linear Low Density Polyethylene/Rice Husk Composites. *Journal of Polymers and the Environment* **2021**, *29*, 1600-1615, https://doi.org/10.1007/s10924-020-01983-6.
39. Lee, S.; Kontopoulou, M.; Park, C. Effect of nanosilica on the co-continuous morphology of polypropylene/polyolefin elastomer blends. *Polymer* **2010**, *51*, 1147-1155, https://doi.org/10.3390/ma13214776.
40. Chen, G-H.; Wu, D-J.; Weng, W-G.; Yan, W-L. Dispersion of graphite nanosheets in a polymer matrix and the conducting property of the nanocomposites. *Polymer Engineering & Science* **2001**, *41*, 2148-2154, https://doi.org/10.1002/pen.10909.
41. Sever, K.; Tavman, I. H.; Seki, Y.; Turgut, A.; Omastova, M.; Ozdemir, I. Electrical and mechanical properties of expanded graphite/high density polyethylene nanocomposites. *Composites Part B: Engineering* **2013**, *53*, 226-233, https://doi.org/10.1016/j.compositesb.2013.04.069.
42. Wang, Y.; Ermilov, V.; Strigin, S.; Safaei, B. Multilevel modeling of the mechanical properties of graphene nanocomposites/polymer composites. *Microsystem Technologies* **2021**, *27*, 4241-4251, https://doi.org/10.1007/s00542-021-05218-z.

43. Chen, G-H.; Wu, D-J.; Weng, W-G.; Yan, W-L. Preparation of polymer/graphite conducting nanocomposite by intercalation polymerization. *Journal of Applied Polymer Science* **2001**, *82*, 2506-2513, https://doi.org/10.1002/app.2101.
44. Fim, F. de C.; Basso, N. R. S.; Graebin, A. P.; Azambuja, D. S.; Galland, G. B. Thermal, electrical, and mechanical properties of polyethylene–graphene nanocomposites obtained by in situ polymerization. *Journal of Applied Polymer Science* **2013**, *128*, 2630-2637, https://doi.org/10.1002/app.38317.
45. Scaffaro, R.; Botta, L. Nanofilled Thermoplastic–Thermoplastic Polymer Blends, In Nanostructured polymer blends. Elsevier, **2014**, 133-160, https://doi.org/10.1016/B978-1-4557-3159-6.00005-5.
46. Krystyjan, M.; Khachatryan, G.; Grabacka, M.; Krzan, M.; Witczak, M.; Grzyb, J.; Woszczak, L. Physicochemical, bacteriostatic, and biological properties of starch/chitosan polymer composites modified by graphene oxide, designed as new bionanomaterials. *Polymers* **2021**, *13*, 2327, https://doi.org/10.3390/polym13142327.
47. Alghdeir, M.; Mayya, K.; Dib, M. Characterization of nanosilica/low-density polyethylene nanocomposite materials. *Journal of Nanomaterials* **2019**, https://doi.org/10.1155/2019/4184351.
48. Upasen, S.; Wattanachai, P. Packaging to prolong shelf life of preservative-free white bread. *Heliyon* **2018**, *4*, e00802, https://doi.org/10.1016/j.heliyon.2018.e00802.
49. Cui, Y.; Kundalwal, S.; Kumar, S. Gas barrier performance of graphene/polymer nanocomposites. *Carbon* **2016**, *98*, 313-333, https://doi.org/10.1016/j.carbon.2015.11.018.
50. Lyn, F. H.; Tan, C. P.; Zawawi, R. M.; Hanani, Z. A. N. Physicochemical properties of chitosan/graphene oxide composite films and their effects on storage stability of palm-oil based margarine. *Food Hydrocolloids* **2021**, *117*, 106707, https://doi.org/10.1016/j.foodhyd.2021.106707.
51. Peter, A.; Mihaly Cozmuta, L.; Nicula, C.; Mihaly Cozmuta, A.; Talasman, C. M.; Drazic, G.; Peñas, A.; Calahorro, A. J.; Sagratini, G.; Silvi, S. Chemical and organoleptic changes of curd cheese stored in new and reused active packaging systems made of Ag-graphene-TiO_2-PLA. *Food Chemistry* **2021**, *363*, 130341, https://doi.org/10.1016/j.foodchem.2021.130341.
52. Khalaj, M-J.; Ahmadi, H.; Lesankhosh, R.; Khalaj, G. Study of physical and mechanical properties of polypropylene nanocomposites for food packaging application: Nano-clay modified with iron nanoparticles. *Trends in Food Science & Technology* **2016**, *51*, 41-48, https://doi.org/10.1016/j.tifs.2016.03.007.
53. Sabet, M.; Soleimani, H. Inclusion of graphene on LDPE properties. *Heliyon* **2019**, *5*, e02053, https://doi.org/10.1016/j.heliyon.2019.e02053.
54. Galdi, M. R.; Nicolais, V.; Di Maio, L.; Incarnato, L. Production of active PET films: evaluation of scavenging activity. *Packaging Technology and Science* **2008**, *21*, 257-268, https://doi.org/10.1002/pts.794.
55. Byun, Y.; Bae, H.J.; Whiteside, S. Active warm-water fish gelatin film containing oxygen scavenging system. *Food hydrocolloids* **2012**, *27*, 250-255, https://doi.org/10.1016/j.foodhyd.2011.06.010.
56. Kuila, T.; Bose, S.; Mishra, A. K.; Khanra, P.; Kim, N. H.; Lee, J. H. Effect of functionalized graphene on the physical properties of linear low density polyethylene nanocomposites. *Polymer Testing* **2012**, *31*, 31-38, https://doi.org/10.1016/j.polymertesting.2011.09.007.
57. Barikloo, H.; Ahmadi, E.; Ahmadi, S. Evaluation of PE/POE/PA6 blends containing silica and clay toward nano composite packaging film. *Journal of Food Measurement and Characterization* **2021**, *15*, 2297-2308, https://doi.org/10.1007/s11694-020-00781-x.
58. Tesarikova, A.; Merinska, D.; Kalous, J.; Svoboda, P. Influence of clay nanofillers on properties of ethylene-octene copolymers. *Polymer Composites* **2018**, *39*, 4581-4593, https://doi.org/10.1002/pc.24568.
59. Gaska, K.; Xu, X.; Gubanski, S.; Kádár, R. Electrical, mechanical, and thermal properties of LDPE graphene nanoplatelets composites produced by means of melt extrusion process. *Polymers* **2017**, *9*, 11, https://doi.org/10.3390/polym9010011.
60. Kamphunthong, W.; Sirisinha, K. Thermal property improvement of ethylene-octene copolymer through the combined introduction of filler and silane crosslink. *Journal of applied polymer science* **2010**, *115*, 424-430, https://doi.org/10.1002/app.31017.
61. Pavlidou, S.; Papaspyrides, C. A review on polymer–layered silicate nanocomposites. *Progress in polymer science* **2008**, *33*, 1119-1198, https://doi.org/10.1016/j.progpolymsci.2008.07.008.
62. Tarani, E.; Papageorgiou, D. G.; Valles, C.; Wurm, A.; Terzopoulou, Z.; Bikiaris, D. N.; Schick, C.; Chrissafis, K.; Vourlias, G. Insights into crystallization and melting of high density polyethylene/graphene nanocomposites studied by fast scanning calorimetry. *Polymer Testing* **2018**, *67*, 349-358, https://doi.org/10.1016/j.polymertesting.2018.03.029.